GEOPHYSICAL AND PALEOSEISMIC INVESTIGATIONS OF LARGE SAND BLOWS ALONG A NORTHWEST-ORIENTED LINEAMENT NEAR MARIANNA, ARKANSAS

Final Technical Report

Research supported by the U.S. Geological Survey (USGS),
Department of the Interior, under award G18AP00083

Principal Investigator
Martitia Tuttle

Co-Principal Investigators
Haydar Al-Shukri and Hanan Mahdi

Other Contributors
Rauf Hussein, Kathleen Dyer- Williams,
and Kathleen Tucker

M. Tuttle & Associates
P.O. Box 345
Georgetown, ME 04548
Tel: 207-371-2007
E-mail: mptuttle@earthlink.net
URL: http://www.mptuttle.com

Project Period: 9/1/2018-3/31/2020

Program Element I: National & Regional Earthquake Hazards Assessments

Key Words: Paleoliquefaction, Paleoseismology, Age Dating

GEOPHYSICAL AND PALEOSEISMIC INVESTIGATIONS OF LARGE SAND BLOWS ALONG A NORTHWEST-ORIENTED LINEAMENT NEAR MARIANNA, ARKANSAS

Principal Investigator
Martitia Tuttle

Co-Principal Investigators
Haydar Al-Shukri and Hanan Mahdi

Other Contributors
Rauf Hussein, Kathleen Dyer- Williams,
and Kathleen Tucker

M. Tuttle & Associates
P.O. Box 345
Georgetown, ME 04548
Tel: 207-371-2007
E-mail: mptuttle@earthlink.net

Abstract

Large sand blows occur along the northwest-oriented Daytona Beach lineament (DBL), which appears to be the surface expression of a fault zone imaged below in seismic reflection profiles. The sand blows formed as the result of large earthquakes circa 4.8, 5.5, and 9.9 thousand years ago (ka), and at least two earlier events between 11 ka and 41 ka, likely produced by rupture of the underlying fault zone. Results of our investigations at three liquefaction sites – DBNW3, DBNW4, and DBNW5 - along the lineament support these interpretations, but also point to the need for more robust dating of Late Pleistocene sand blows in order to better understand the Marianna paleoearthquake chronology prior to 10 ka and the long-term behavior of the fault zone. No sand blow that formed during the 6.8 ka event, recorded by a compound sand blow northeast of Marianna, has yet been found along the Daytona Beach lineament, though that could change with additional investigations. Previously, liquefaction potential analysis indicated that earthquakes in the moment magnitude (**M**) range of 6-6.5 produced by the fault zone could have induced liquefaction in the study area. Analysis performed during this study indicates that larger Marianna earthquakes would be required to induce liquefaction at distal sites where features are similar in age to the Marianna earthquakes. A Marianna earthquake in the **M** 7.2-7.5 range could account for a small sand blow northwest of Blytheville, Arkansas, and sand dikes east of Tunica, Mississippi, that are similar in age to the 4.8 ka event; a Marianna earthquake in the **M** 6.9-7.5 range could account for a small sand blow and related dikes northwest of Marked Tree, Arkansas, that are similar in age to the 5.5 ka event; and a Marianna earthquake in the **M** 6.3-7.0 range could explain a small sand blow and sand dikes east of Tunica, Mississippi, that are similar in age to the 6.8 ka event. On the basis of our current knowledge, the fault zone beneath the DBL repeatedly produced large earthquakes between 4.8 and 9.9 ka with recurrence times ranging from 700 – 4,400 years. The Marianna source may have been seismically active for at least 36 thousand years (kyr) between 4.8 ka and 41 ka before entering its current apparently quiescent period.

Introduction

Paleoliquefaction studies provide information about the timing, location, magnitude, and recurrence times of large paleoearthquakes (e.g., Obermeier, 1996; Tuttle, 2001; Tuttle et al., 2019a). This type of information is crucial for assessing earthquake hazard in regions such as the Central and Eastern United States where active faults rarely rupture the ground surface or are otherwise difficult to recognize. For the New Madrid seismic zone (NMSZ), 1811-1812-type earthquake sequences, or New Madrid events, were recognized in A.D. 1450 ± 150 yr, A.D. 900 ± 150 yr, A.D. 0 ± 200 yr, 1050 ± 250 yr B.C., and 2350 ± 150 yr B.C., primarily through the study of sand blows (Figure 1; e.g., Tuttle et al., 2002, 2005, 2019b and 2019c). From these paleoseismic data, mean recurrence times were estimated of 500 years between A.D. 900 and A.D. 1811 and of 1,100 years between 2350 B.C. and A.D. 900 for New Madrid events.

In the Marianna area, where only a few small earthquakes have been recorded during the instrumental period, very large sand blows were found west and southwest of the town of Marianna in the Western Lowlands and northeast of Marianna in the St. Francis Basin (Figures 1 and 2; Al-Shukri et al., 2005, 2006; Tuttle et al., 2006). Most of the sand blows have deeply weathered profiles suggesting that they are thousands of years old. Radiocarbon and optically-stimulated luminescence (OSL) dating methods were used to estimate ages of the sand blows. None of the sand blows formed less than 4.8 ka or are similar in age to known New Madrid events. In the St. Francis Basin, a compound sand blow exposed in the St. Francis drainage ditch and buried beneath back-swamp deposits likely formed as the result of a sequence of large earthquakes about 6.8 ka (Figures 1 and 2). In the Western Lowlands, large sand blows concentrated along, but not limited to, a northwest-oriented lineament, referred to as the Daytona Beach lineament (DBL), formed about 4.8, 5.5, 9.9 ka and between 11 ka and 41 ka, probably as the result of large earthquakes produced by an underlying fault zone (Figures 2 and 3). At two of the sites (DBSE2 and DBNW2) along the DBL, soft-sediment faults were observed crosscutting sand dikes and soil lamellae that had developed in the dikes. The soft-sediment faults are parallel to the DBL as well as the feeder dikes, suggesting that emplacement of the sand dikes was fault-controlled (Tuttle et al., 2006; Al-Shukri et al., 2015). Initial liquefaction potential analysis suggested that earthquakes of **M** 6-6.5, if produced by the DBL and located 5-10 km below the sand blows, could account for liquefaction at the sites (Al-Shukri et al., 2015). Consequently, **M** 6-6.5 was considered a minimum magnitude estimate for Marianna paleoearthquakes.

Seismic reflection surveys that crossed the DBL imaged near-vertical faults in the 100-1000-m-depth range, which likely includes Eocene through Paleozoic strata (Odum et al., 2016). The DBL and associated sand blows coincide with the imaged faults below. The geophysical study also found that fault displacements increases with depth, suggesting long-term recurrent faulting. These findings support the interpretation that the DBL and associated sand blows are the surface expression of a fault zone that produced repeated large-magnitude earthquakes (RLMEs) in the past (Tuttle et al., 2006; Al-Shukri et al., 2009, 2015).

During paleoliquefaction studies in the NMSZ, small sand blows (10-25 cm thick) and related sand dikes were found at the Eaker 2 site northwest of Blytheville, Arkansas, and at the Promised Land site near Ditch 10 northwest of Marked Tree, Arkansas, that are similar in age (4.8 and 5.5 ka, respectively) to large sand blows in the Marianna area (Tuttle et al., 2019b). These sand

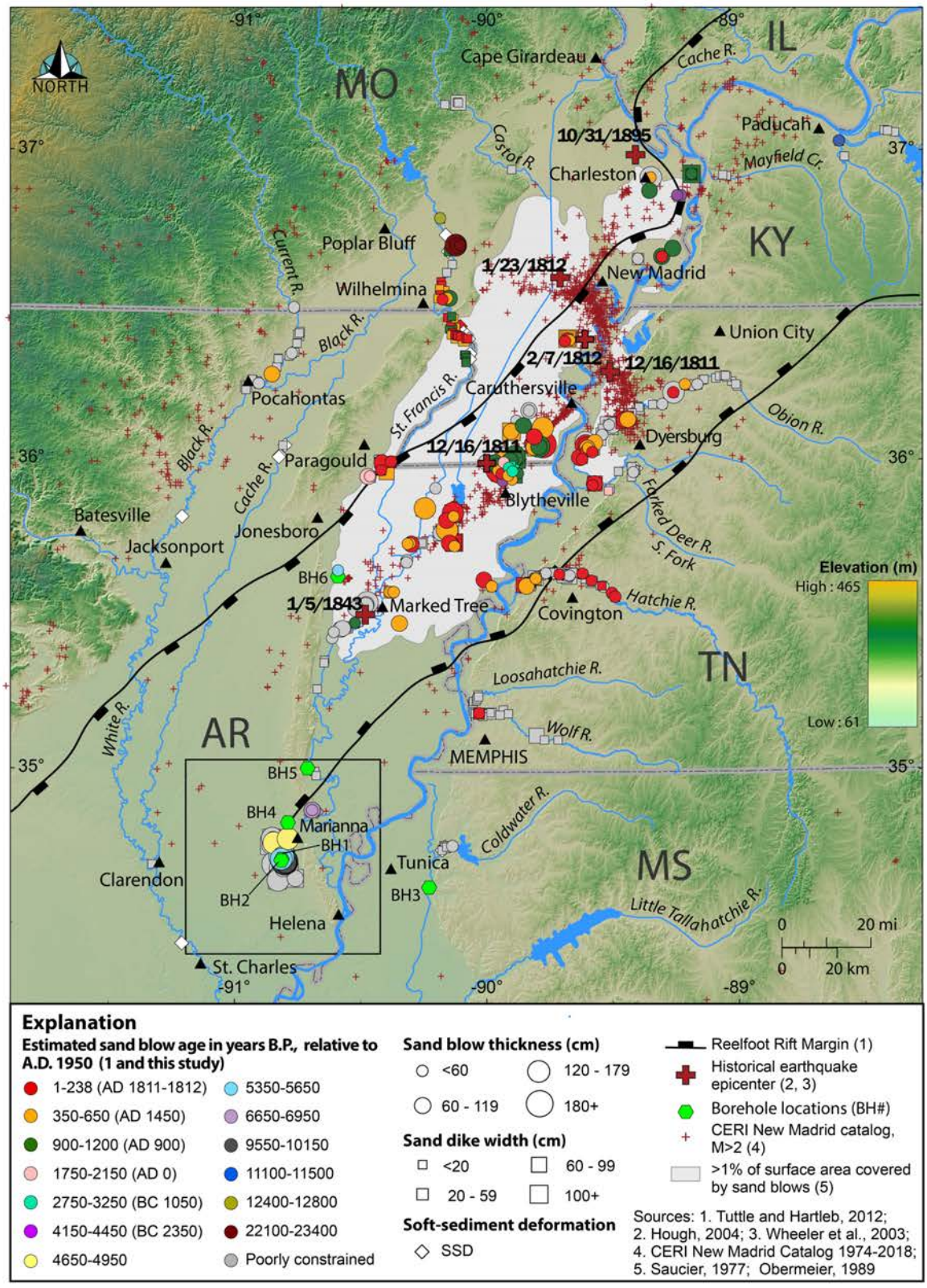

Figure 1. Shaded relief map of NMSZ (delineated by seismicity) and Marianna area (outlined by black square) showing locations, measured sizes, and estimated ages of earthquake-induced liquefaction features. The Marianna area is located near the southern end of the eastern Reelfoot Rift margin.

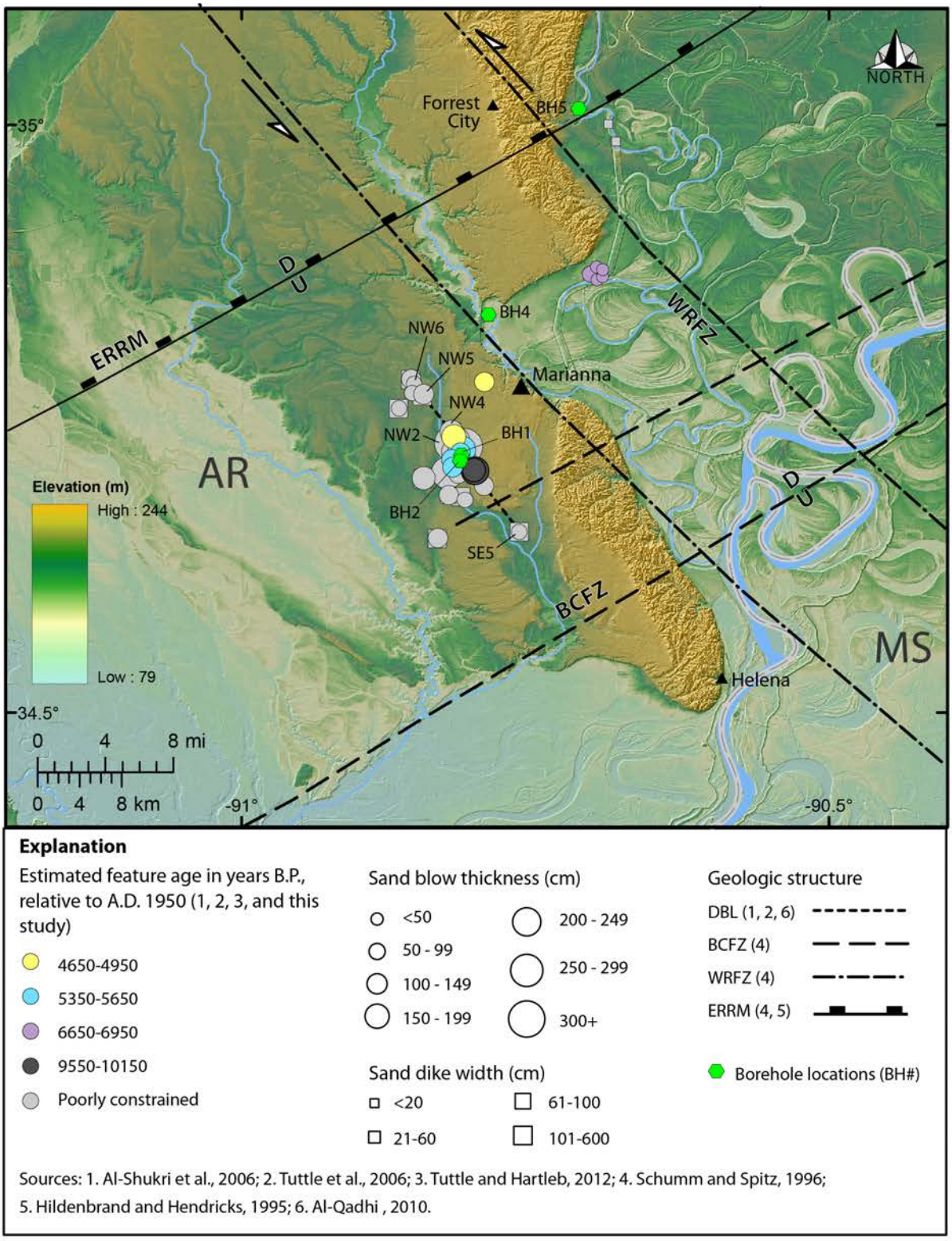

Figure 2. Shaded relief map of Marianna area showing locations, measured sizes, and estimated ages of sand blows and dikes studied during this and previous NEHRP grants. Note that the DBL (short dashed line) is in close proximity and about 5 km west of the White River fault zone (WRFZ). Other mapped faults in the area include the Big Creek fault zone (BCFZ) and eastern Reelfoot Rift Margin (ERRM).

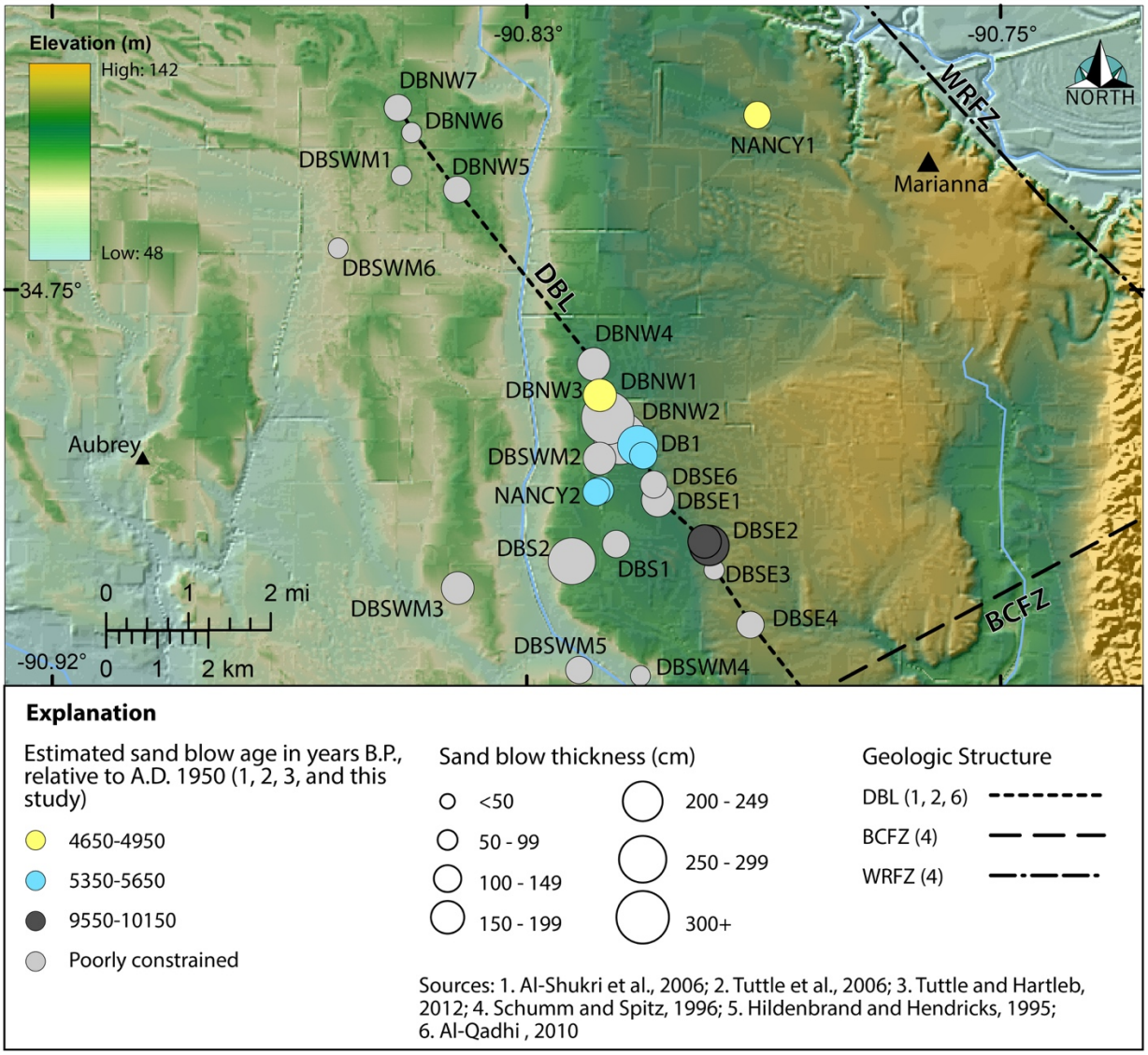

Figure 3. Shaded relief map of DBL showing locations, measured sizes, and estimated ages of sand blows studied during this and previous NEHRP grants. During this study, geophysical and paleoseismic investigations were conducted at the sites DBNW3 and DBNW5, and begun at DBNW4, where paleoseismic trenches could not be excavated due to a high-water table.

blows are older and smaller than sand blows attributed to New Madrid paleoearthquakes. Therefore, these small sand blows may represent distal features resulting from large Marianna earthquakes (Figure 1). According to the relation between earthquake magnitude and farthest distance to surface effects of liquefaction (Ambraseys, 1988; Castilla and Audemard, 2007), an earthquake produced by the Marianna source below the DBL would have to be of **M** ≥ 6.9 to produce sand blows at the Promised Land site 105 km away and **M** ≥ 7.2 to produce sand blows at the Eaker 2 site 140 km away (Figure 4).

During a recent paleoliquefaction project in the NMSZ and surrounding region, three generations of liquefaction features were discovered along the Coldwater River east of Tunica, Mississippi (Figure 1). Two generations of the features overlap the ages (4.8 ka and 6.8 ka) of large

Marianna sand blows, and therefore, may have formed as the result of Marianna earthquakes (Tuttle et al., 2019b). The liquefaction features along the Coldwater River are relatively small, which is consistent with the interpretation that they are distal features related to large Marianna earthquakes. According to the magnitude-distance relation (Ambraseys, 1988; Castilla and Audemard, 2007), an earthquake produced by the Marianna source below the DBL would have to be of **M** ≥ 6.3 to produce liquefaction features at the most distant Coldwater sites, 62 km away (Figure 4).

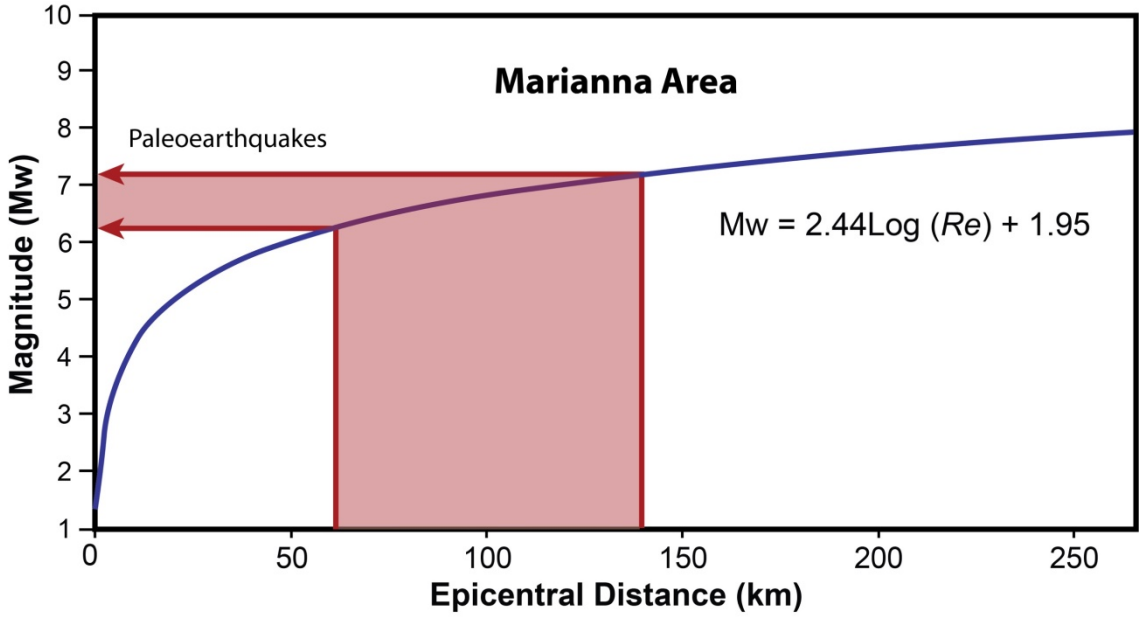

*Figure 4. Relation between moment magnitude (**M**w) and epicentral distance (Re) to farthest liquefaction effects in very susceptible sediment developed from worldwide data (modified from Castilla and Audemard, 2007). According to the relation, a **M**≥ 6.9 Marianna paleoearthquake could induce liquefaction 105 km away, the distance of paleoliquefaction features at Promised Land site; a **M** ≥ 7.2 Marianna paleoearthquake could induce liquefaction 140 km away, the distance of paleoliquefaction features at Eaker 2 site; and a **M** ≥ 6.3 could induce liquefaction 62 km away, the greatest distance of paleoliquefaction features documented along Coldwater River.*

The sand blows and sand dikes along the DBL are very large and their source sands relatively deep (>12.5 m). Therefore, it seems likely that the earthquakes responsible for their formation are large to very large in magnitude. Very large earthquakes would be expected to induce liquefaction at considerable distances in sediments that tend to be susceptible to liquefaction such as Holocene fluvial deposits. Therefore, it is reasonable to interpret the relatively small sand blows and sand dikes at the Promised Land, Eaker 2, and Coldwater sites that are similar in age to Marianna events as distal liquefaction features. If these features are part of liquefaction fields for the 4.8 ka, 5.5 ka, and 6.8 ka Marianna events, there are large geographical gaps in those liquefaction fields. Additional reconnaissance, investigations, and dating of liquefaction features in northwestern Mississippi, and east-central Arkansas, would help to better define the size and areal distribution of similar-age features across the region and to fill the geographical gaps in the liquefaction fields related to Marianna events.

This study focuses on measuring and dating large sand blows along the northwest-oriented DBL,

further documenting its history of activity, and evaluating scenario earthquakes that could account for distal liquefaction features, thus constraining the magnitudes of Marianna events.

Paleoseismic Investigations

Paleoseismic investigations were originally scheduled for late October-early November 2018, following the harvest of crops. However, the fall of 2018 was exceedingly rainy, leading to flooding of rivers, drainage ditches, and fields in the Marianna area. At times it was impossible to reach the sites even with a four-wheel drive. At other times, it was possible to reach the sites but the soils were too wet for ground-penetrating radar (GPR) surveys and for excavation of paleoseismic trenches. The fields and our study sites remained very wet through the spring and early summer 2019. As a result, field work was delayed until October-early November 2019 to follow the harvest. GPR surveys were conducted at several sites, including Daytona Beach Northwest 3 (DBNW3), Daytona Beach Northwest 4 (DBNW4), and Daytona Beach Northwest 5 (DBNW5). Based on the GPR results, we sited paleoseismic trenches at the three sites. In late October 2019, we excavated two trenches each at DBNW3 and DBNW5 only to have it rain 6-7 cm twice in a week, leading to flooding of the trenches, partial collapse of three of the trenches, and total collapse of the fourth trench. With nearly continuous pumping, we manage to drain, muck out, and log three of the trenches. Because the water table was so high after the torrential rainstorms, water continued to flow along the contacts between the sand blows and underlying buried soils towards the sand dikes and into the trenches, threatening to undermine the trench walls. We had to buttress the walls with sediment and mud to prevent their collapse and to temporarily uncover them to log the walls. Because of the rain and resulting high-water table, excavation of paleoseismic trenches at DBNW4 was canceled. With the apparent shift to rainy weather earlier in the fall, future field work will be scheduled in September and early October. This change in the field schedule will precede the fall harvest, which may limit the fields where we can get permission to work and will necessitate paying farmers for crop damage.

Daytona Beach Northwest 3 (DBNW3) Site

The DBNW3 site is located along the DBL about 1.2 km northwest of the original Daytona Beach site (DB1) (Figure 3; Tuttle et al., 2006). This site was chosen for study because it occurs along the lineament and is in close proximity to DBNW2 where sand blows likely to be Late Pleistocene in age were destroyed by sand mining, prohibiting their further study. Based on interpretation of satellite imagery and field reconnaissance, including excavation of soil pits, we identified a sandy deposit that was likely to be a sand blow (Figure 5). We selected an area of 50 m by 90 m for GPR survey to map the likely sand blow and to identify its feeder dikes.

Over the course of fourteen months, we surveyed the site several times under different soil moisture conditions with an average of 15 profiles per survey, covering the area where the apparent sand blow is visible at the surface (Figure 5). Profile lengths average 82 meters and each profile consists of about 4,100 scans (one scan every 2 centimeters). The range (nanoseconds) was set such that the penetrating depth was about 1.5 to 1.8 meters in order to image in detail the sand blow and related sand dikes. From the GPR data, two-dimensional (2-D) images of the profiles were created. For example, 2-D images of profiles 23 and 22 are shown in Figure 6. The strong reflector shown by the red and blue bands represents the contact between sand (the sand blow) and underlying silt (soil of the buried pre-event ground surface).

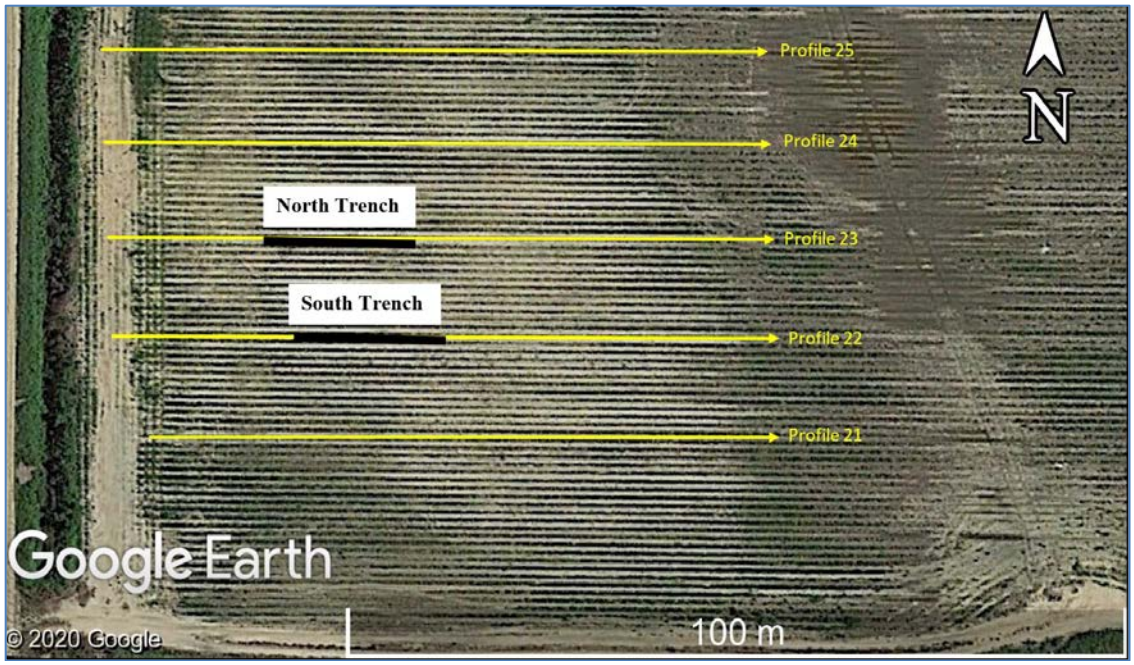

Figure 5. Google Earth image of site DBNW3 showing the northwest-southeast elongated sand blow (light-colored soils), locations of ground-penetrating radar (GPR) profiles 21, 22, 23, 24, and 25 (yellow lines), and locations of two paleoseismic trenches (heavy black lines).

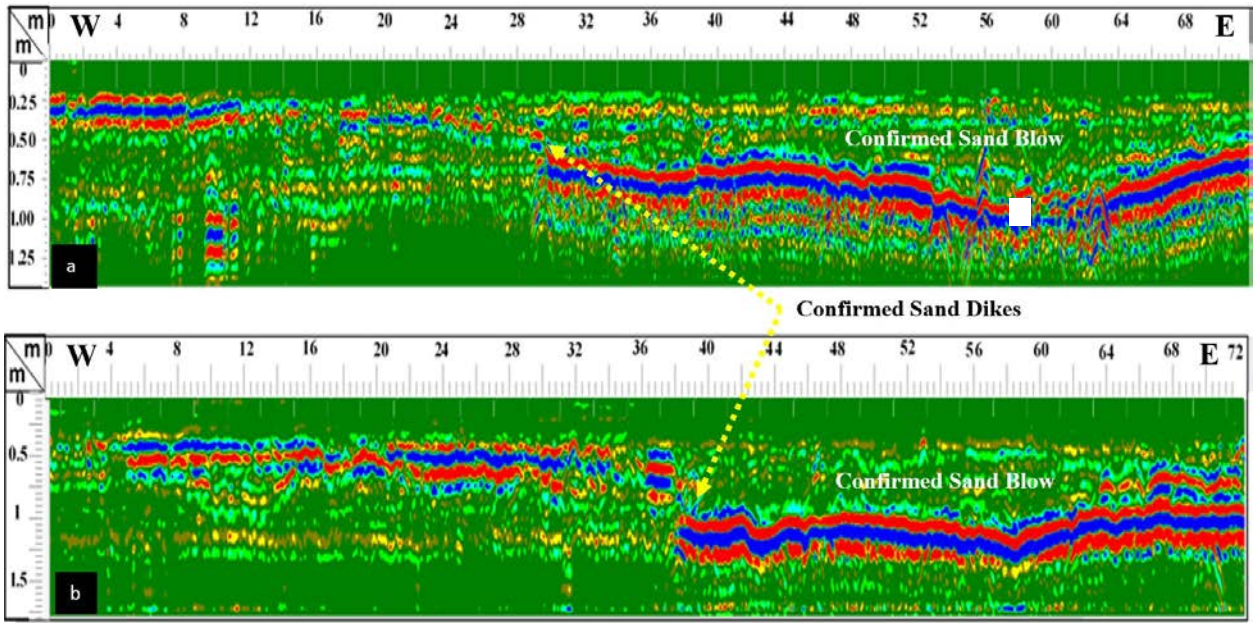

Figure 6. GPR profiles 23 (a) and 22 (b) show deformation of a strong reflector (red and blue bands) which represents the contact between the sand blow above and buried silty soil below. Discontinuities in the contact are related to ground failure and sand dikes.

In both profiles, there is a break in, and vertical offset across, the strong reflector that represent a breach in and vertical displacement of the buried surface. A displacement of ~20 cm can be seen in profile 23 at meter mark 30 and of ~40 cm in profile 22 at meter mark 38. In both profiles, the buried surface has been displaced downward on the east side of the breach. The break in the strong reflector, and thus the breach in the buried soil, likely represents the feeder dike through which water and entrained sand vented onto the pre-event surface to form the sand blow. In profile 23, other breaks in the strong reflector occur at meter mark 38 as well as between meter marks 52 and 62 and likely reflect other sand dikes.

Two trenches were excavated along GPR profiles 23 and 22 to verify the presence of a sand blow and related sand dikes, to study characteristics of the sand blow, and to collect samples for OSL and radiocarbon dating. The trenches were parallel to one another and extended only about 10 m east of the main dike in order to remain a safe distance from a nearby gas pipeline. The portions of the trenches that revealed the main feeder dikes were logged at the scale of 1" = 50 cm (Figures 7 and 8).

As observed in the trenches, the sand blow was more than 24-m wide and up to 80-cm thick. The main sand dike had an average strike and dip of N40°W, 81°NE (not all measurements are shown in Figures 7 and 8) and was 17 cm wide in the northern trench and up to 100 cm wide in the southern trench. A small (4 cm wide) feeder dike, with a strike and dip of N41°W, 87°NE, was also found about 4 m east of the main dike in the northern trench. The pre-event ground surface was displaced downward on the northeast side of the dike by ~10 cm in the northern trench and ~40 cm in the southern trench. Weathering of the sand blow and dike, including the formation of small Fe-Mn nodules and soil lamellae, indicates that they are prehistoric in age. Sediment and organic samples were collected for OSL and radiocarbon dating, respectively. In the northern trench, OSL1 collected from the buried silty soil and OSL3 collected from the clayey silty subsoil yielded ages of 4,495-4,925 yr B.P. and 12,770-13,850 yr B.P., respectively (Figure 7; Table 1). C1 collected from the base of the buried silty soil yielded a calibrated age of 4,528-4,815 yr B.P. (Table 2). The ages of OSL1 and C1 are very similar and provide close maximum constraining ages of 4,815 yr B.P. and 4,925 yr B.P. for the sand blow and related sand dikes. In the southern trench, C1 collected from the upper part of the sand blow just below the plow zone gave a calibrated age of 0-304 yr B.P. This age is very young suggesting that the sample was of a tree root or some other plant material recently incorporated in the top of the sand blow. OSL1 collected from the clayey silty subsoil yielded an age of 12,095-12,905 yr B.P., similar to the age of the subsoil in the northern trench.

The OSL and radiocarbon ages of the buried soil indicate that the liquefaction features at this site formed soon after 4,815-4,925 yr B.P., probably during the 4.8 ka earthquake. The OSL ages of the subsoil indicate that the sediment was deposited more than 12 ka and that the overlying soil had been forming *in situ* for about 8 kyr prior to burial by the sand blow.

Daytona Beach Northwest 5 (DBNW5) Site

The DBNW5 site is located along the DBL about 5.9 km northwest of the original DB1 (Figure 3; Tuttle et al., 2006). This site was selected for investigation because it is farther north than most of the sites we have studied so far and the apparent sand blow at the site appears to be

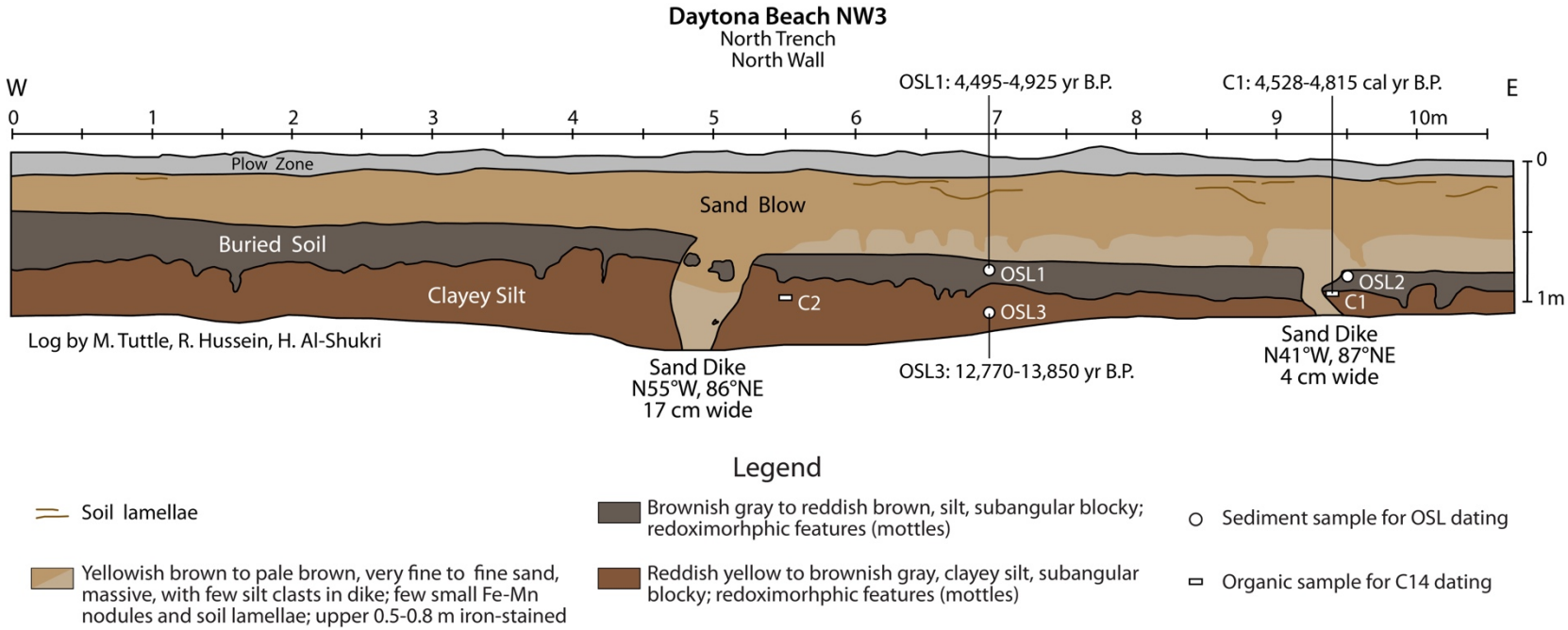

Figure 7. Log of the north wall of the northern trench excavated in the sand blow at site DBNW3. The trench was excavated along the transect of GPR profile 23 (see Figures 5 and 6) and shows a cross-section of the sand blow, sand dikes, and buried soils, as well as the positions of OSL and radiocarbon samples. OSL and radiocarbon dating of the buried soils provides close maximum constraining ages for the sand blow and related sand dikes and indicate that they formed about 4.8 ka. Note that the upper 0.5-0.8 m of the sand blow is weathered (indicated by light brown shading) and includes small Fe-Mn nodules and soil lamellae.

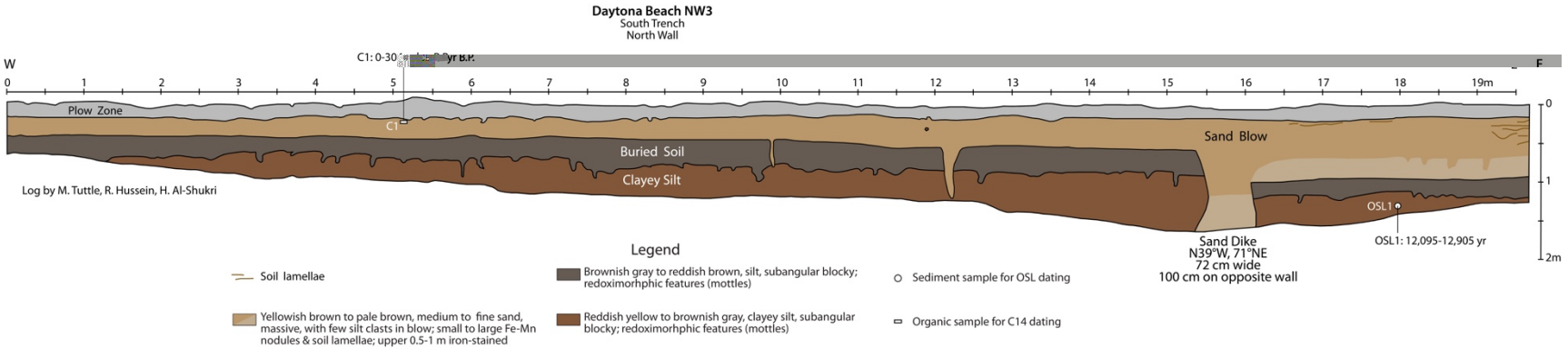

Figure 8. Log of the north wall of the southern trench excavated in the sand blow at site DBNW3. The trench was excavated along the transect of GPR profile 22 (see Figures 5 and 6) and shows a cross-section of the sand blow, sand dikes, and buried soils, as well as the positions of OSL and radiocarbon samples. OSL date of the buried subsoil (OSL1) agrees with the date of the buried subsoil (OSL3) in the northern trench. The organic sample (C1) collected immediately below the plow zone from the upper part of the sand blow is very young and probably was from a root recently grown into the sand blow from above. As in the northern trench, the upper 0.5-0.8 m of the sand blow is weathered (indicated by light brown shading) and includes small Fe-Mn nodules and soil lamellae.

Table 1. Results of optically-stimulated luminescence ages on quartz grains, single aliquot regeneration.

Sample DB Lab #	Depth (m)	Cosmic Dose Rate (mGray/yr)[1]	Dose Rate (mGray/yr)	OSL Age Yr[2]	Age Yr B.P.[3]	Sample Description
NW3-NTR-OSL1 BG4884	0.7	0.18 ± 0.02	2.69 ± 0.06	4770 ± 215	4,495-4,925	north wall; collected 3-5 cm below sand blow from buried silty soil
NW3-NTR-OSL3 BG4885	1.1	0.17 ± 0.02	2.69 ± 0.07	13,370 ± 540	12,770-13,850	north wall; collected 33-38 cm below sand blow from clayey silty subsoil
NW3-STR-OSL1 BG4886	1.3	0.17 ± 0.02	3.16 ± 0.07	12,560 ± 405	12,095-12,905	north wall; collected 32-37 cm below sand blow from clayey silty subsoil
NW5-STR-OSL1 BG4894	0.53	0.21 ± 0.02	3.15 ± 0.03	13,950 ± 1330	12,560-12,220	north wall; collected 3-5 cm below sand blow from buried silty soil
NW5-STR-OSL2 BG4895	0.77	0.19 ± 0.02	3.41 ± 0.08	17,080 ± 635	16,385-17655	north wall; collected 25-30 cm below sand blow from silty subsoil

[1] Cosmic dose rate calculated from parameters in Prescott and Hutton (1994) and includes soft component (Peng and Forman, 2019 at https://www.baylor.edu/geosciences/index.php?id=962356).

[2] Systematic and random errors calculated in a quadrature at one standard deviation by the luminescence dating and age calculator (Peng and Forman, 2019 at https://www.baylor.edu/geosciences/index.php?id=962356). Datum year is A.D. 2010.

[3] Years B.P. or before present (A.D. 1950).

Table 2. Results of radiocarbon dating.

Sample DB Beta Lab-#	$^{13}C/^{12}C$ Ratio	Conventional Radiocarbon Age Yr B.P.[1]	Probability %	Calibrated Radiocarbon Age Yr B.P.[2]	Calibrated Calendar Date A.D./B.C.[2]	Sample Description
NW3N-C1 546853	-24.1	4120 ± 30	70.3 25.1	4726-4528 4815-4753	2777-2579 BC 2866-2804 BC	Charred; collected 12-15 cm below sand blow from buried soil
NW3S-C1 546854	-23.8	210 ± 30	50.5 30.8 14.1	216-144 304-266 21-Post BP 0	AD 1734-1806 AD 1646-1684 AD 1929-Post 1950	Charred; from upper 5 cm of sand blow
NW5S-C1 546855	-24.3	710 ± 30	84.8 10.6	694-644 588-565	AD 1256-1306 AD 1362-1385	Organic sediment; from tree root cast in upper part of sand blow

[1] Conventional radiocarbon ages in years B.P. or before present (1950) determined by Beta Analytic, Inc. Errors represent 1 standard deviation statistics or 68% probability.

[2] Calibrated age ranges as determined by Beta Analytic, Inc., using the high probability density range method: INTCAL13 (Bronk Ramsey, 2009; Reimer et al., 2013). Ranges represent 2 standard deviation statistics or 95% probability.

exceptionally large. The sand blow was identified on satellite imagery and confirmed as a likely sand blow during field reconnaissance, including excavation of soil pits (Figure 9).

We conducted GPR surveys several times at this site. It was difficult to get a good image of the subsurface because the water table tends to be very shallow. In early October 2019, when the water table was lower than normal, we collected eleven high-resolution profiles. Transects of five of the profiles, shown on Figure 9, have average lengths of 60 meters. Two profiles, not shown on Figure 9, were 200 meters long. All the profiles were collected in the east-west direction and showed a strong reflector indicative of a contact between sand (the sand blow) and underlying silty clay (soil of the buried old surface).

Figure 10 shows profiles 44 (upper) and 43 (lower) in which a strong reflector is clearly visible as well as three breaks in the reflector. The depth of the strong reflector indicates that the sand blow is at least 1-m thick and the breaks in the reflector are indicative of feeder dikes. Although

they are separated by only 15 meters, the two profiles show substantial differences in the locations and widths of the feeder dikes. The widths of the dikes in the southern profile are apparently much greater than the widths of the dikes in the northern profile. The largest and westernmost dike in the two trenches appears to occur about 4 m farther west in the northern profile than it does in the southern profile, suggesting that the main feeder dike is oriented northwest – southeast.

Two trenches were excavated along the same transects as GPR profiles 44 and 43 and revealed a very large sand blow and related feeder dikes (Figure 9). Unfortunately, two storms resulting in a total of 14 cm of rain flooded the trenches, leading to partial collapse of the southern trench and total collapse of the northern trench. By almost continuous pumping of the trench and by buttressing its walls, we managed to log the north wall of the southern trench and to collect samples for dating (Figure 11). The sand blow was more than 16-m wide, up to 140-cm thick, and buried a silty, clay soil. The main sand dike was about 270-cm wide and had an approximate strike of N45°W. The buried soil was displaced downward by about 110 cm on the northeast side of the dike. Several large clasts of silty clay occurred in the sand blow above the feeder dike. In GPR profile 43, reflections off these large clasts gave the appearance of intact soil cut by two sand dikes. However, in the trench, we could see that there was one very wide dike contained large clasts of the buried soil instead. The sand blow was very weathered and characterized by a zone of small to medium Fe-Mn nodules in its upper 40 cm and large nodules above its basal contact with the buried soil. The degree of weathering suggests that the liquefaction features at this site are more than a few thousand years old.

Organic sample C1 collected from a tree root cast that had formed in the top of the sand blow gave a calibrated age of 565-694 yr B.P. (Figure 11; Table 2). This represents a minimum, but probably not a close minimum, constraining age of 565 yr B.P. Sediment sample OSL1 collected near the top of the buried silty clay soil yielded an age of 12,560-15,220 yr B.P. and provides a maximum constraining age of 15,220 yr B.P. for the sand blow and related sand dikes (Figure 11; Table 1). OSL2 collected about 24 cm below OSL1 gave an age of 16,385-17,655 yr B.P.

The OSL age of the buried soil indicates that the liquefaction features at this site formed after 15,220 yr B.P. The OSL age of the subsoil indicate that the sediment was deposited more than 16 ka and that the overlying soil had been forming *in situ* for 1-4 kyr prior to burial by the sand blow. If the sand blow formed about 13.9 $\pm$ 1,330 ka, it does not correspond to any known Marianna event. The sand blow is closest in age to the upper sand blow at DBSE2, which is thought to have formed ~9.9 ka based on maximum constraining ages of the soil buried by the sand blow, including a radiocarbon age of 9.9 ka $\pm$ 300 yr and an OSL age of 12 ka $\pm$ 1000 yr. Given the similarity in the OSL ages of their buried soils, it seems possible that the liquefaction features at DBNW5 formed during the same event as the upper sand blow at DBSE2. However, additional dating is needed at DBNW5 to better constrain the age of the sand blow and to determine if it is related to the 9.9 ka event or an event during the Late Pleistocene.

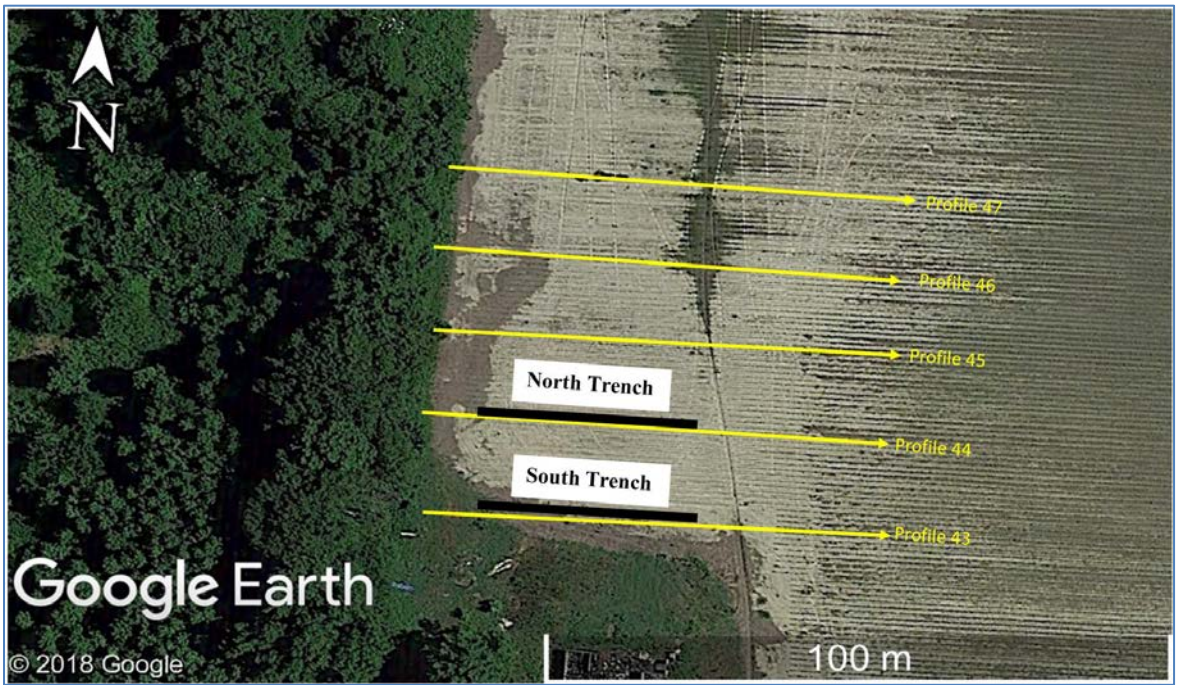

Figure 9. Google Earth image of site DBNW5 showing a very large sand blow (light-colored soils), locations of ground-penetrating radar (GPR) profiles 43, 44, 45, 46, and 47 (yellow lines), and locations of two paleoseismic trenches (heavy black lines).

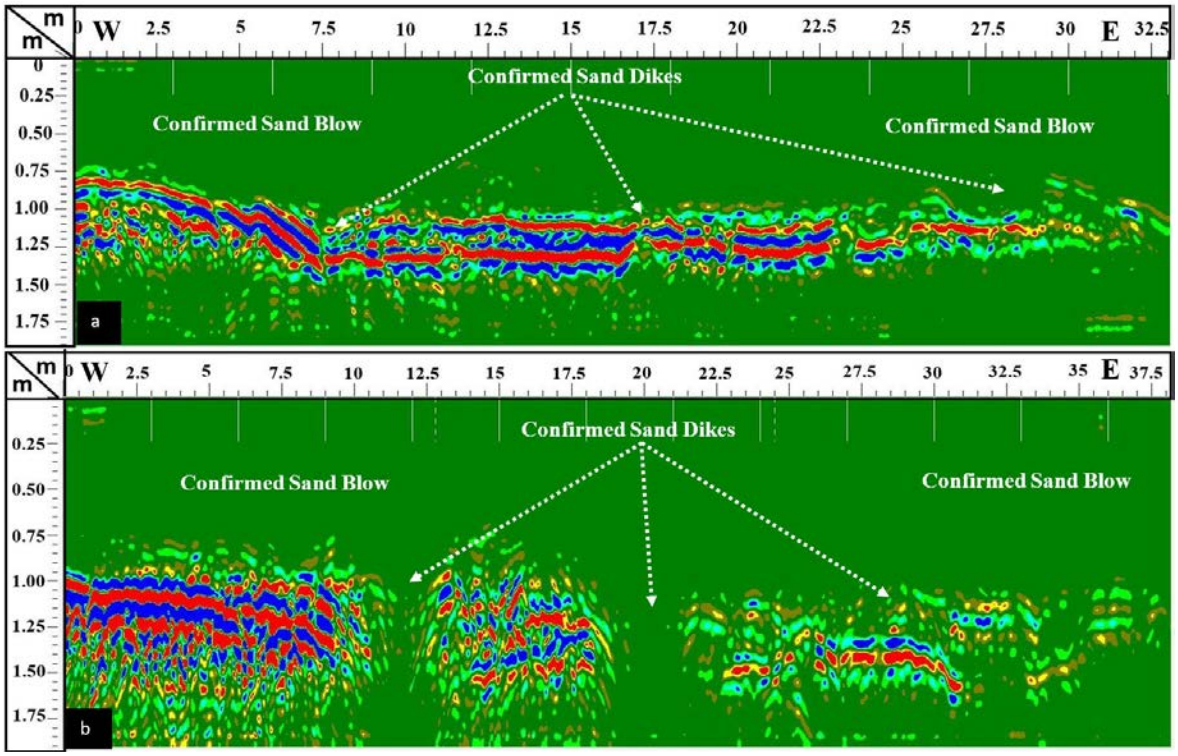

Figure 10. GPR profiles 44 (a) and 43 (b) show deformation of a strong reflector (red and blue bands) which represents the contact between the sand blow above and buried silty soil below. Discontinuities in the contact are related to ground failure and sand dikes.

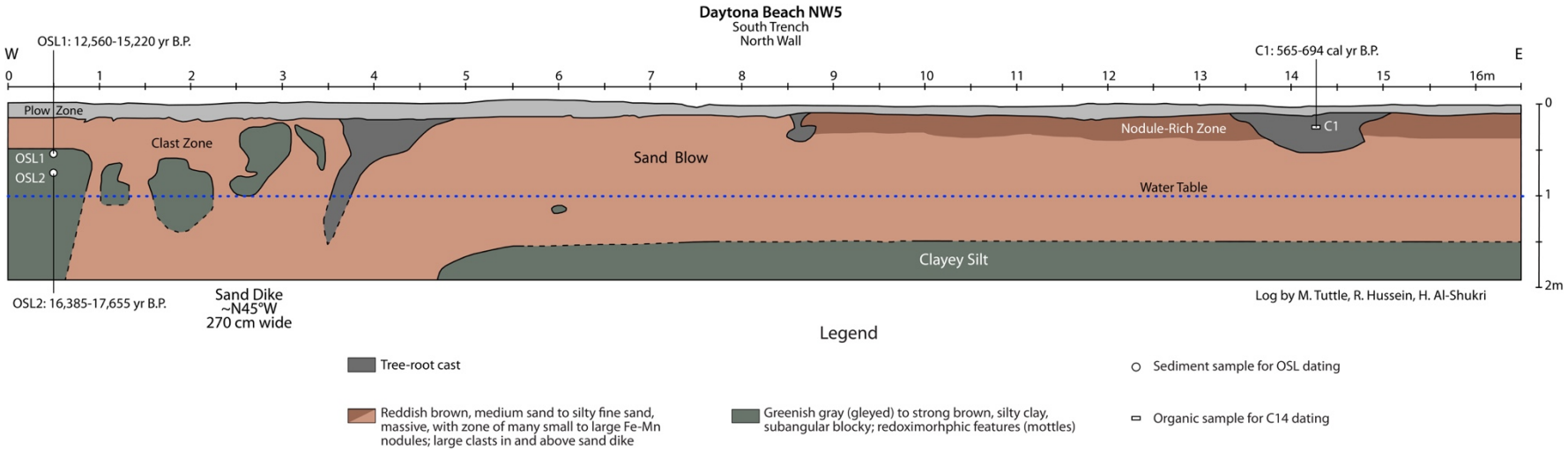

Figure 11. Log of the north wall of the southern trench excavated in the sand blow at site DBNW5. The trench was excavated along the transect of GPR profile 43 (see Figures 5 and 6) and shows a cross-section of the sand blow, sand dike, and buried soil, as well as the positions of OSL and radiocarbon samples. OSL date of the buried soil (OSL1) provides a maximum constraining age of 12,560-15,220 yr B.P. The organic sample (C1) from a tree root cast in the top of the sand blow is young but provides a minimum constraining age of 565-694 yr B.P. The sand blow was very weathered and included a zone of small Fe-Mn nodules in the upper part of the sand blow and also large nodules in the lower part of the sand blow. Large clasts of the silty clay were concentrated in the sand blow above the feeder dike. The high-water table (dotted blue line) and buttressed trench walls made it difficult to log the contact between the sand blow and underlying soil (dashed where inferred).

Daytona Beach Northwest 4 (DBNW4) Site

The DBNW4 site is located along the DBL about 1.8 km northwest of DB1 (Figure 3; Tuttle et al., 2006). This site was chosen for study because it occurs along the lineament and, like DBNW3, is in close proximity to DBNW2 where sand blows likely to be Late Pleistocene in age were destroyed by sand mining. Based on interpretation of satellite imagery and field reconnaissance, including excavation of soil pits, we identified a sandy deposit that was likely to be a sand blow (Figure 12). We selected an area of 100 m by 150 m for GPR survey to map the likely sand blow and its feeder dikes.

GPR surveys were conducted in the fall of 2018 and again in the fall of 2019. Both surveys consisted of about ten, east-west oriented profiles that were between 110 meters and 148 meters long. The range (nanoseconds) was such that the penetrating depth was about 1.8 meters and the scan rate was 50 scans per meter. Figure 12 shows the locations of five of the 2019 GPR profiles in the immediate vicinity of the likely sand blow. As can be seen in GPR profile 35, a strong reflector representing the contact between the sand blow and underlying soil suggests that the sand blow is about 0.8-m thick and that the contact is fairly flat-lying for at least 40 meters (Figure 13). Between the 17.5- and 20-meter marks of the profile, there is a 2.5-m-wide break in the reflector that probably represents that main feeder dike. As suggested by deformation of the reflector at the 27.5-meter mark, there may be another dike about 7.5 m east of the main dike. On the basis of these observations, we planned to excavate a paleoseismic trench along the same transect as GPR profile 35 (Figure 12).

As mentioned in the beginning of this section, two rain storms within one week flooded many of the fields and drainage ditches in our study area. At this site, the paleoseismic trench was not excavated prior to the rain storms. After the storms and problems with flooding and collapsing trenches at DBNW3 and DBNW5, we dug a soil pit to monitor the water level at DBNW4. During the week following the rain storms, the water level fell from ~40 cm to ~70 cm below the surface but never got below the base of the sand blow. Having lost one trench and struggled to work around partial trench collapses at the other two sites, we knew it would be imprudent to excavate the planned trench while the water table was above the contact between the sand blow and buried soil. When another rainstorm was forecast and it was clear that the rainy season had begun, we canceled excavation of the sand blow at DBNW4. We hope to be able to excavate the sand blow in the future when the water table is below the base of the sand blow.

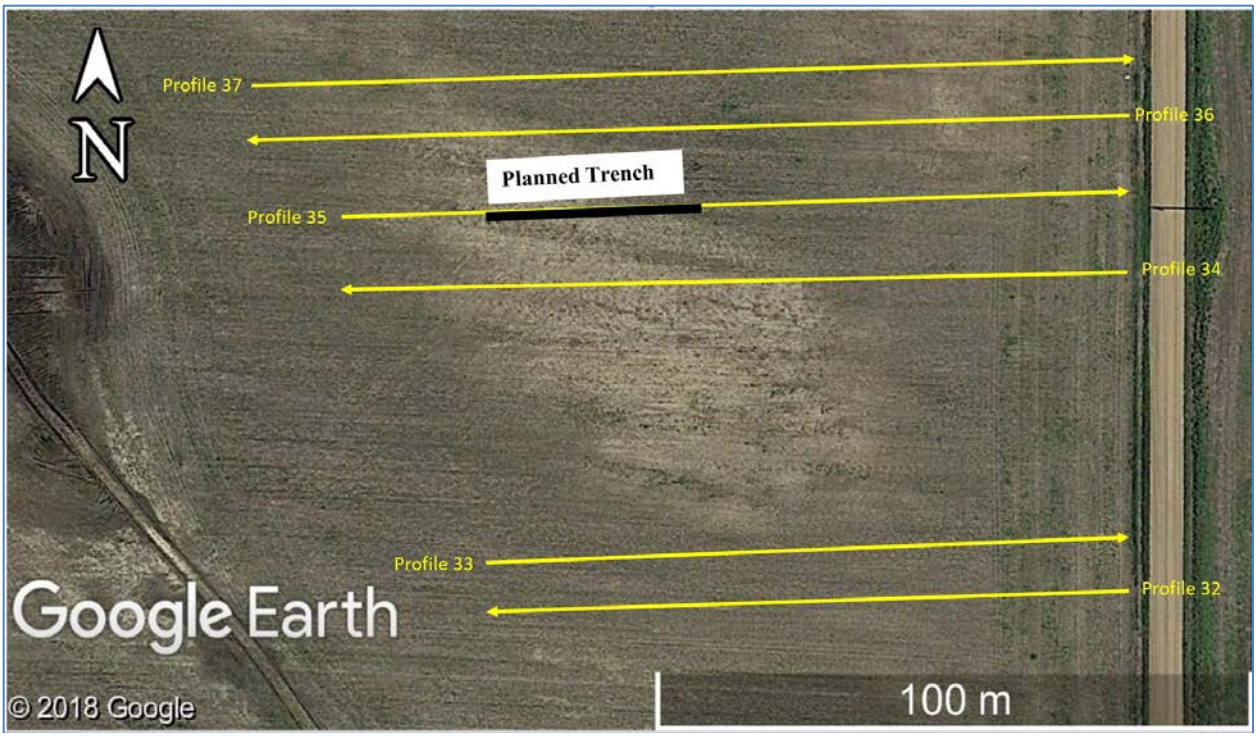

Figure 12. Google Earth image of site DBNW4 showing the northwest-southeast elongated sand blow (light-colored soils), locations of ground-penetrating radar (GPR) profiles 32, 33, 34, 35, 36, and 37 (yellow lines), and location of the planned trench (heavy black line).

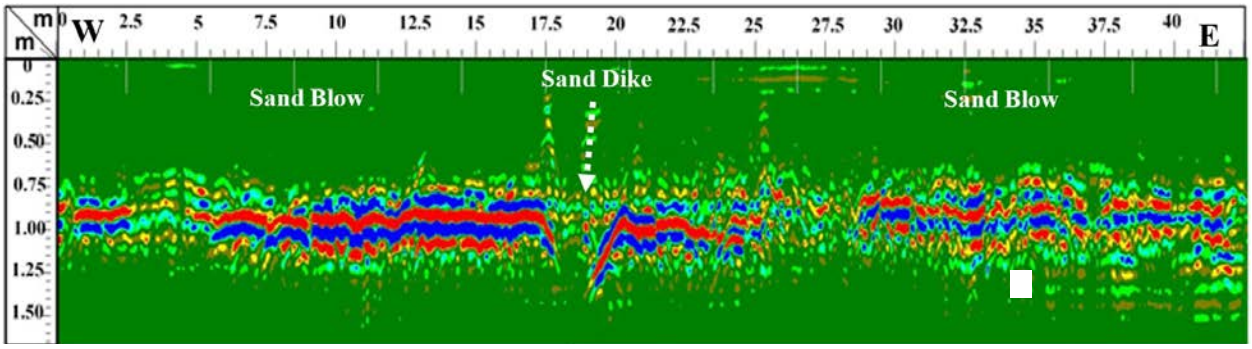

Figure 13. GPR profile 35 shows deformation of a strong reflector (red and blue bands), representing the contact between the sand blow above and buried silty soil below, and the 2.5-m-wide break in the contact, which is likely to be the main sand dike.

Evaluation of Scenario Earthquakes

Previously, we evaluated scenario earthquakes using liquefaction potential analysis in order to estimate the magnitude of Marianna earthquakes that produced large sand blows in our study area (Al-Shukri et al., 2015). The fault zone imaged below the DBL, and along which large sand blows formed, was assumed to be the earthquake source. Cone-penetration testing data collected by the U.S. Geological Survey at Lee 1 and Lee 3 sites within several hundreds of meters of two of the liquefaction sites, DB1 and Nancy 2, near the DBL was used in the analysis (Figure 3 and

Table 3). The evaluation indicated that local earthquakes in the **M** 6-6.5 range could induce liquefaction in sandy sediment that occurs ≥ 12.5 m below the surface. The magnitude estimate was viewed as a minimum value since the study only consider very localized effects.

Table 3. Locations of geotechnical data used in previous studies.

Borehole Locations (Map ID)	Distance from Fault Zone (km)	Latitude Dec. Degrees	Longitude Dec. Degrees	Location Description
Lee 1 (1)	5, 10	34.71860°	-90.81944°	Lee County Road 337, southwest of Marianna
Lee 3 (2)	5, 10	34.71381°	-90.82032°	Lee County Road 337, southwest of Marianna
Coldwater River (3)	55	34.62956°	-90.23040°	Route 3 bridge over Coldwater River, west of Savage, MS

As mentioned in the Introduction, three generations of liquefaction features were discovered along the Coldwater River in northwestern Mississippi, during a regional paleoliquefaction study. The two older generations of features are similar in age to Marianna sand blows, and therefore, may have formed as the result of Marianna earthquakes (Figure 1; Tuttle et al., 2019b). Standard penetration test (SPT) data that was collected by the Mississippi Department of Transportation at a bridge crossing of the Coldwater River downriver from the liquefaction sites was used in the analysis (Table 3). Evaluation of scenario earthquakes found that a **M** 6.7 Marianna earthquake was unlikely to induce liquefaction ~55 km away along the Coldwater River; a **M** 7.0 Marianna event might produce marginal liquefaction; and a **M** 7.5 event was likely to produce widespread liquefaction in the area.

In this study, we evaluated additional scenario earthquakes to further constrain the magnitudes of Marianna earthquakes that would be required to induce liquefaction at distal sites where features similar in age to Marianna sand blows have been found. SPT data was used in the analysis that was collected by the Arkansas Department of Transportation at bridge crossings of the L'Anguille River north of Marianna (13 km from the fault zone), the St. Francis River near Madison (37 km from the fault zone), and Ditch 10 near Promised Land (105 km from the fault zone) near documented liquefaction sites (Figures 1 and 2; Table 4). The data were reviewed and cohesionless sandy sediments within 20 m of the ground surface and with blow counts of less than 30 were selected for analysis. Based on the water table depths observed in the boreholes and the likelihood that the water table was deeper at the time of the Marianna paleoearthquakes than it is today, we considered sediment at 5 m or more below the ground surface. Description of sediment at those borehole locations, including the sediment depth and blow counts used in the liquefaction potential analysis described below, are provided in Table 5.

Table 4. Locations of geotechnical data used in this study.

Borehole Locations (Map ID)	Distance from Fault Zone (km)	Latitude Dec. Degrees	Longitude Dec. Degrees	Location Description
L'Anguille River (4)	13	34.83779	-90.79641	Highway 1 bridge, northwest of Marianna
St. Francis River (5)	37	35.01297	-90.71929	Highway 50 bridge, east of Madison
Ditch 10 (6)	105	35.63440	-90.60272	County Road 48 bridge, southwest of Trumann

Table 5. Description of sediment used in liquefaction potential analysis.

Site Name Borehole No. (Map ID)	Depth (m)	Description of Susceptible Sediment	Blow Count (N)[1]
L'Anguille River	9	wet, medium dense, gray sand	19
BH 4	11	wet, medium dense, gray sand	19
(4)	12	moist, medium dense gray sand	25
	14	wet, medium dense gray sand	18
	15	wet, very loose, gray sand with clay seams	3
St. Francis River	5	moist, loose, brown sand with some clayseams	7
BH 1	6	wet, loose, brown sand	7
(5)	8	moist, loose, brown sand	7
	9	wet, very loose, gray silty sand	2
	14	wet, medium dense, gray sand	16
	15	wet, medium dense, gray sand	15
Ditch 10	9	wet, medium dense sand with traces of organic matter	17
BH 1	12	wet, medium dense, gray sand	13
(6)	14	wet, medium dense, gray sand	20
	17	wet, medium dense, gray sand	12

Liquefaction Potential Analysis

Scenario earthquakes were evaluated using the cyclic stress method, also known as the simplified procedure, for assessing liquefaction potential (e.g., Seed and Idriss, 1971 and 1982; Youd et al., 2001 and 2003; Cetin et al., 2004; Idriss and Boulanger, 2004; Moss et al., 2006; Robertson, 2004 and 2009). First, we estimated peak ground accelerations (PGA) that would be generated by scenario earthquakes of various moment magnitudes (**M** 5.5, 6.0, 6.5, 7.0 and 7.5) at distances (13, 37, and 105 km) of the geotechnical sites located near distal liquefaction features. Regionally appropriate, medium ground motion prediction equations (GMPEs) (Atkinson and Boore, 2011; Atkinson et al., 2012; Atkinson and Assatourians, 2012) were used to calculate

[1] Blow count (N) is the total number of blows required to drive a split spoon sampler 0.3 m using standard hammer (63.5 kg) dropping 0.76 m and is a measure of soil or sediment relative density.

PGA. After determining the accelerations, cyclic stress ratios (CSR) generated by scenario earthquakes were calculated using Equation 1:

$$CSR_{7.5} = \frac{\tau_{ave}}{\sigma'_{vo}} = 0.65 \cdot \left(\frac{a_{max}}{g}\right) \cdot \left(\frac{\sigma_{vo}}{\sigma'_{v0}}\right) \cdot r_d \cdot \frac{1}{MSF} \quad (1)$$

where a_{max}=PGA (horizontal component), (a_{max}/g) is PGA divided by the acceleration due to gravity; σ_{vo} and σ'_{v0} are the total and effective vertical overburden stresses, respectively; r_d is a stress reduction coefficient; and MSF is the magnitude scaling factor. The $CSR_{7.5}$ represents the normalized shear stress (τ_{ave}/σ_v) induced in the soil by the earthquake event (i.e., the seismic demand) and commonly referenced to a benchmark case with **M** = 7.5.

Variations in the SPT procedure were corrected by adjusting the measured blow count (N_m) to 60% of the potential energy using Equation 2:

$$\boldsymbol{N_{1(60)} = C_N\, C_E\, C_B\, C_R\, C_S\, N_m} \quad (2)$$

where $N_{1(60)}$ is normalized blow count corrected for hammer energy (C_E), effective confining stress (C_N), borehole diameter (C_B), rod length (C_R), and sampler configuration (C_S), with N_m being the measured SPT resistance or "blow count" reported in blows/foot (or blows/0.3m). The correction factors and blow counts were derived from the borehole logs.

Following the computations of the cyclic stress ratio and the adjusted and normalized blow count, the liquefaction potential of representative layers at borehole sites were determined. The CSR for a scenario earthquake was plotted against the normalized blow count $(N_1)_{60}$ for the site (Seed and Idriss, 1971). If the point plots on or above the base curve, a lower bound of liquefaction for **M** 7.5 earthquakes, the soil is likely to liquefy. Conversely, if the point plots below the curve, liquefaction is considered unlikely.

In this study, we elected to use an approximation to the base curve, the cyclic resistance ratio (CRR), which lends itself to ease of use in spreadsheets. As proposed by Youd et al. (2001), the CRR for an **M** 7.5 event in clean sand was calculated using Equation 3:

$$CRR_{7.5} = \frac{1}{34 - (N_1)_{60-cs}} + \frac{(N_1)_{60-cs}}{135} + \frac{50}{\left[10 \cdot (N_1)_{60-cs} + 45\right]^2} - \frac{1}{200} \quad (3)$$

for $(N_1)_{60\text{-}cs} < 30$; $(N_1)_{60\text{-}cs}$ refers to equivalent clean sand.

If CSR is greater than or equal to CRR, the soil is likely to liquefy. Conversely, if CSR is less than CRR, liquefaction is considered unlikely.

The CRR for an earthquake with magnitudes other than 7.5 was calculated by multiplying $CSR_{7.5}$ by the appropriate magnitude scaling factor (MSF), which is given by Equation 4 where M_w represents moment magnitude:

$$MSF = (M_w/7.5)^{-3.3} \quad (4)$$

We used the following equation to calculate the value of the CRR to be used in the evaluation of scenario earthquakes with magnitudes other than 7.5:

$$CRR = CRR_{M7.5} * MSF \quad (5)$$

Once the CSR and the CRR were calculated, we determined the factor of safety against liquefaction (FS_L) using the following equation:

$$FS_L = \frac{CRR}{CSR} \quad (6)$$

The calculated factor of safety (FS) was then be used to approximately assess the probability of liquefaction (P_L). For example, in their approach, Juang and Jiang (2000) suggested (Eq. 7):

$$P_L = \frac{1}{1 + (FS / 1.0)^{3.34}}, \quad (7)$$

where P_L is the probability of liquefaction and *Fs* is the factor of safety. If P_L is greater than or equal to 50%, a layer is likely to liquefy.

Results

The results of the evaluation of Marianna scenario earthquakes are discussed below. Details of liquefaction potential analysis for scenario earthquakes of **M** 5.5, 6.0, 6.5, 7.0 and 7.5 are presented in Tables 6, 7, 8, 9, and 10. These new results as well as previous results are summarized in Table 11.

Table 6. Results of liquefaction potential analysis for M 5.5 Marianna scenario earthquake.

Site Name (Map ID)	Distance (km)	Depth (m)	a_{max}[1] Medium	$N_{1(60)}$[2]	Cyclic Stress Ratio[3]	Results[4]
L'Anguille River (4)	13	9	0.26	20	0.201	N
	13	11	0.26	19	0.205	N
	13	12	0.26	23	0.205	N
	13	14	0.26	16	0.200	N
	13	15	0.26	3	0.195	L
St. Francis River (5)	37	5	0.08	9	0.051	N
	37	6	0.08	8	0.055	N
	37	8	0.08	8	0.060	N
	37	9	0.08	2	0.064	N
	37	14	0.08	15	0.064	N
	37	15	0.08	13	0.062	N

[1] a_{max} = Maximum acceleration at ground surface

[2] $N_{1(60)}$ = Corrected blow count (N) from the standard penetration test (SPT)

[3] Cyclic Stress Ratio = Shear stress induced in soil by earthquake

[4] N = Liquefaction not likely; L = Liquefaction likely

Table 7. Results of liquefaction potential analysis for M 6.0 Marianna scenario earthquake.

Site Name (Map ID)	Distance (km)	Depth (m)	a_{max}[1] Medium	$N_{1(60)}$[2]	Cyclic Stress Ratio[3]	Results[4]
L'Anguille River (4)	13	9	0.43	20	0.335	N
	13	11	0.43	19	0.343	L
	13	12	0.43	23	0.342	N
	13	14	0.43	16	0.334	L
	13	15	0.43	3	0.325	L
St. Francis River (5)	37	5	0.13	9	0.083	N
	37	6	0.13	8	0.091	N
	37	8	0.13	8	0.099	N
	37	9	0.13	2	0.105	N
	37	14	0.13	15	0.105	N
	37	15	0.13	13	0.102	N

[1] a_{max} = Maximum acceleration at ground surface

[2] $N_{1(60)}$ = Corrected blow count (N) from the standard penetration test (SPT)

[3] Cyclic Stress Ratio = Shear stress induced in soil by earthquake

[4] N = Liquefaction not likely; L = Liquefaction likely

Table 8. Results of liquefaction potential analysis for M 6.5 Marianna scenario earthquake.

Site Name (Map ID)	Distance (km)	Depth (m)	a_{max}[1] Medium	$N_{1(60)}$[2]	Cyclic Stress Ratio[3]	Results[4]
L'Anguille River (4)	13	9	0.67	20	0.523	L
	13	11	0.67	19	0.536	L
	13	12	0.67	23	0.535	L
	13	14	0.67	16	0.522	L
	13	15	0.67	3	0.508	L
St. Francis River (5)	37	5	0.21	9	0.131	N
	37	6	0.21	8	0.144	L
	37	8	0.21	8	0.157	L
	37	9	0.21	2	0.166	L
	37	14	0.21	15	0.167	N
	37	15	0.21	13	0.161	N
Ditch 10 (6)	105	9	0.05	18	0.038	N
	105	12	0.05	12	0.039	N
	105	14	0.05	18	0.038	N
	105	17	0.05	10	0.035	N

[1] a_{max} = Maximum acceleration at ground surface

[2] $N_{1(60)}$ = Corrected blow count (N) from the standard penetration test (SPT)

[3] Cyclic Stress Ratio = Shear stress induced in soil by earthquake

[4] N = Liquefaction not likely; L = Liquefaction likely

Table 9. Results of liquefaction potential analysis for M 7.0 Marianna scenario earthquake.

Site Name (Map ID)	Distance (km)	Depth (m)	a_{max}[1] Medium	$N_{1(60)}$[2]	Cyclic Stress Ratio[3]	Results[4]
Ditch 10 (6)	105	9	0.10	18	0.082	N
	105	12	0.10	12	0.084	N
	105	14	0.10	18	0.082	N
	105	17	0.10	10	0.076	N

[1] a_{max} = Maximum acceleration at ground surface

[2] $N_{1(60)}$ = Corrected blow count (N) from the standard penetration test (SPT)

[3] Cyclic Stress Ratio = Shear stress induced in soil by earthquake

[4] N = Liquefaction not likely; L = Liquefaction likely

Table 10. Results of liquefaction potential analysis for M 7.5 Marianna scenario earthquake.

Site Name (Map ID)	Distance (km)	Depth (m)	a_{max}[1] Medium	$N_{1(60)}$[2]	Cyclic Stress Ratio[3]	Results[4]
Ditch 10 (6)	105	9	0.16	18	0.126	N
	105	12	0.16	12	0.129	L
	105	14	0.16	18	0.127	N
	105	17	0.16	10	0.117	L

[1] a_{max} = Maximum acceleration at ground surface

[2] $N_{1(60)}$ = Corrected blow count (N) from the standard penetration test (SPT)

[3] Cyclic Stress Ratio = Shear stress induced in soil by earthquake

[4] N = Liquefaction not likely; L = Liquefaction likely

Considering scenario earthquakes produced by the Marianna source, a **M** 5.5 earthquake would not induce liquefaction even at the local geotechnical sites, Lee 1 and Lee 3 (Tables 6 and 11); however, a **M** 6.0 located 5 km below Lee 1 and Lee 3, would induce liquefaction at those sites and also at the L'Anguille River site (Tables 7 and 11). A **M** 6.5 earthquake located 10 km below Lee 1 and Lee 3, would induce liquefaction at those sites, the L'Anguille River site, and the St. Francis River site (Tables 8 and 11). A **M** 7.0 earthquake would induce marginal liquefaction at the Coldwater River site, but not at the Ditch 10 site (Tables 9 and 11). It would take a **M** 7.5 earthquake to induce liquefaction at the Ditch 10 site as well as the Coldwater River site (Tables 10 and 11).

As discussed in the Introduction, a Marianna paleoearthquake about 4.8 ka produced very large sand blows along the DBL, and possibly a small sand blow northwest of Blytheville, Arkansas, and sand dikes along Coldwater River east of Tunica, Mississippi. If so, this event may have been of **M** ≥ 7.2 according to the magnitude-distance relation and possibly as large as **M** 7.5

Table 11. Summary of evaluation of Marianna scenario earthquakes.

Site Name	Map ID	Distance (km)	Results[1]	Observed
1. Scenario earthquake M 5.5				
Lee 1	1	5	N	L
Lee 1	1	10	N	L
Lee 3	2	5	N	L
Lee 3	2	10	N	L
L'Anguille River	4	13	N	L
St. Francis River	5	37	N	L
2. Scenario earthquake M 6.0				
Lee 1	1	5	L	L
Lee 1	1	10	N	L
Lee 3	2	5	L	L
Lee 3	2	10	N	L
L'Anguille River	4	13	L	L
St. Francis River	5	37	N	L
3. Scenario earthquake M 6.5				
Lee 1	1	5	L	L
Lee 1	1	10	L	L
Lee 3	2	5	L	L
Lee 3	2	10	L	L
L'Anguille River	4	13	L	L
St. Francis River	5	37	L	L
Coldwater River	3	55	N	L
Ditch 10	6	105	N	L
4. Scenario earthquake M 7.0				
Coldwater River	3	55	L/N	L
Ditch 10	6	105	N	L
5. Scenario earthquake M 7.5				
Coldwater River	3	55	L	L
Ditch 10	6	105	L	L

[1]Liquefaction likely for 45% - 100% of the layers analyzed; L/N = marginal because liquefaction predicted for 24% - 44% of the layers analyzed; N = liquefaction not likely because liquefaction predicted for less than 24% of the layers analyzed.

according to liquefaction potential analysis. A Marianna paleoearthquake about 5.5 ka produced very large sand blows along the DBL and possibly a small sand blow and related dikes near Ditch 10 northwest of Marked Tree, Arkansas. If so, this event may have been of **M** ≥ 6.9 according to the magnitude-distance relation and possibly as large as **M** 7.5 according to liquefaction potential analysis. In addition, a Marianna paleoearthquake about 6.8 ka produced very large sand blows along the St. Francis Ditch north of Marianna and possibly a small sand blow and sand dikes along the Coldwater River in Mississippi. If so, this event may have been of **M** ≥ 6.3 according to the magnitude-distance relation or of **M** ≥ 7.0 according to liquefaction potential analysis. It is not surprising that magnitude estimates based on liquefaction potential analysis are greater than those derived from the magnitude-distance relation. Liquefaction potential analysis uses blow counts (related to soil density and liquefaction susceptibility) measured at geotechnical sites near the observed paleoliquefaction features; whereas, the magnitude-distance relation is developed from a worldwide database of earthquakes that induced liquefaction in very susceptible sediment (Ambraseys, 1988; Castilla and Audemard, 2007). Magnitude estimates of paleoearthquakes derived from the magnitude-distance relation are considered minimum values.

There are large geographical gaps in the distribution liquefaction features of similar age in the Marianna source area, northwest of Blytheville, Arkansas, northwest of Marked Tree, Arkansas, and east of Tunica, Mississippi. The relatively small sizes liquefaction features near Blytheville, Marked Tree, and Tunica are consistent with the interpretation that they are distal features. However, we would be more confident in this interpretation if a broader distribution of similar age features could be demonstrated. Additional reconnaissance for and dating of liquefaction features in east-central Arkansas, and northwestern Mississippi, as well as further evaluation of scenario earthquakes would help to better assess locations and magnitudes of paleoearthquakes in this region.

Conclusions

Paleoliquefaction features, including large and weathered sand blows and related sand dikes, indicate RLMEs in the Marianna area during the Middle-Early Holocene and Late Pleistocene. Based on investigations of liquefaction features concentrated in the Marianna area, as well as those discovered along the St. Francis Ditch in Arkansas, paleoearthquakes occurred about 4.8, 5.5, 6.8, and 9.9 ka and at least twice between 11 ka and 41 ka. No liquefaction features have been found in the Marianna area that formed during the past 4.8 kyr, when the New Madrid seismic zone, located 80-280 km to the northeast, produced RLMEs. Many large Marianna sand blows define a northwest-oriented lineament, named the DBL, that likely represents the surface expression of an active fault zone. The long axes of the sand blows, their main feeder dikes, and soft-sediment faults that crosscut the dikes are all northwest-oriented and subparallel to the lineament. The DBL is relatively straight, and though discontinuous, can be traced for at least 12 km. Seismic reflection surveys imaged faults below the lineament and found increasing fault displacement with depth, suggesting long-term recurrent faulting.

During this research grant, we investigated three large sand blows along the DBL ranging from 1.2 to 5.9 km northwest of the original Daytona Beach site, DBL1. At the DBNW3 site, the sand blow is up to 80-cm thick; the main feeder dike is up to 100-cm wide and oriented northwest-

southeast; and the pre-event ground surface is displaced vertically, northeast side down, at least 41 cm across the dike. The sand blow was weathered including the formation of small Fe-Mn nodules and soil lamellae. OSL and radiocarbon dating of the soil buried by the sand blow indicates that the liquefaction features at this site formed soon after 4,815-4,925 yr B.P., probably during the 4.8 ka earthquake. At the DBNW5 site, the sand blow is up to 140-cm thick and contains large clasts above the main feeder dike; the main feeder dike is up to 270-cm wide and oriented northwest-southeast; and the pre-event ground surface is displaced vertically, northeast side down, at least 110 cm across the dike. The sand blow was very weathered including a zone of small to medium Fe-Mn nodules in the upper part of the sand blow and large nodules in the lower part of the sand blow. OSL dating of the soil buried by the sand blow indicates that the liquefaction features at this site formed after 15,220 yr B.P. Given the similarity in the OSL age of the buried soils at DBSE2, the liquefaction features at DBNW5 may have formed during the same event as DBSE2 ~9.9 ka. Additional dating is needed at DBNW5 to better constrain the age of the sand blow and to determine if it is related to the 9.9 ka event or to an event during the Late Pleistocene. At DBNW4, the sand blow is up to 80-cm thick; the main feeder dike is up to 250 cm wide and oriented northwest-southeast; and the pre-event ground surface does not appear to be displaced vertically across the sand dike. The age of the sand blow has not yet been estimated because a high-water table prohibited safe excavation of a paleoseismic trench to examine the sand blow and collect samples for dating. The results of our investigations at the three liquefaction sites support the interpretation that the DBL marked by large sand blows is the surface expression of a fault zone that produced RLMEs during the Middle-Early Holocene and Late Pleistocene.

Previously, liquefaction potential analysis indicated that earthquakes in the moment magnitude, **M**, range of 6-6.5 produced by the fault zone beneath the DBL could have induced liquefaction in the study area. Analysis performed during this study indicates that larger Marianna earthquakes would be required to induce liquefaction at distal sites where features are similar in age to the Marianna earthquakes. A Marianna earthquake in the **M** 7.2-7.5 range could account for a small sand blow northwest of Blytheville, Arkansas, and sand dikes along Coldwater River east of Tunica, Mississippi, that are similar in age to the 4.8 ka event; a Marianna earthquake in the **M** 6.9-7.5 range could account for a small sand blow and related dikes near Ditch 10 northwest of Marked Tree, Arkansas, that are similar in age to the 5.5 ka event; and a Marianna earthquake in the **M** 6.3-7.0 range could explain a small sand blow and sand dikes along the Coldwater River east of Tunica, Mississippi, that are similar in age to the 6.8 ka event.

The Marianna paleoearthquake chronology is still poorly understood for the Late Pleistocene and may not yet be complete for the Holocene. On the basis of our current knowledge, however, the fault zone beneath the DBL clearly produced RLMEs between 4.8 ka and 9.9 ka with recurrence times ranging from 700 – 4,400 years. The Marianna source may have been seismically active for at least 36 kyr between 4.8 ka and 41 ka before entering its current apparently quiescent period. If so, this behavior may have implications for the New Madrid seismic zone which began a seismically active period about 4.3 ka, soon after the Marianna source went quiet. Future paleoliquefaction studies in the area will help to improve the Marianna paleoearthquake chronology during the Holocene and Late Pleistocene, to identify the source of the Marianna earthquake ~6.8 ka, and to further evaluate periodicity and migration of seismicity in the region.

Acknowledgments

The Arkansas Department of Transportation and Mississippi Department of Transportation provided geotechnical data used in the liquefaction potential analysis for scenario earthquakes. Kathy Tucker updated the regional paleoliquefaction database and the Marianna and regional maps showing liquefaction sites, mapped faults, and topography. Beta Analytic, Inc. performed radiocarbon dating of organic samples and Steve Forman of Geoluminescense Dating Research Laboratory at Baylor University preformed the OSL dating of sediment samples. Zamara Fuentes and Martha Kopper assisted with geological field work. Thanks to the property owners and farmers who gave us permission to carry out field work at the study sites southwest of Marianna, Arkansas. The material presented in this report is based upon work supported by the U.S. Geological Survey under Grant No. G18AP00083.

References Cited

Ambraseys, N.N., 1988, Engineering Seismology: earthquake engineering and structural dynamics, Journal of the International Association of Earthquake Engineering, v. 17, p. 1-105.

Atkinson, G., and Boore, D., 2011, Modification to existing ground-motion prediction equations in light of new data, Bulletin of the Seismological Society of America, v. 101, n. 3, p. 1121-1135.

Atkinson, G., (with input from) Adams, J., Rogers, G., Onur, T., and Assatourians, K., 2012, White paper on development of ground motion prediction equations for Canadian national seismic hazard maps, www.seismotoolbox.ca (Miscellaneous Resources*)*.

Atkinson, G., (Project Leader), Assatourians, K., 2012, GMPEs for national hazard maps, *www.seismotoolbox.ca* (Miscellaneous resources).

Boulanger, R. W., and Idriss, I. M., 2012, Probabilistic standard penetration test-based liquefaction: triggering procedure, Journal of Geotechnical and Geoenvironmental Engineering, v. 138, n. 10, p. 1185-1195.

Bronk Ramsey, C., 2008, Bayesian analysis of radiocarbon dates, Radiocarbon, v. 51, n. 1, p. 337-360.

Castilla, R.A., and Audemard, F.A., 2007, Sand blows as a potential tool for magnitude estimation of pre-instrumental earthquakes, Journal of Seismology, v. 11, p. 473-487.

Cetin, K. O., Seed, R. B., Der Kiureghian, A., Tokimatsu, K., Harder, L. F. Jr, Kayen, R. E., Moss, R. E. S., 2004, SPT-based probabilistic and deterministic assessment of seismic soil liquefaction potential, ASCE Journal of Geotechnical and Environmental Engineering, v. 130, n. 12, p. 1314-1340.

Forman, S.L., Pierson, J., and Lepper, K., 2000, Luminescence Geochronology, Quaternary Geochronology: Methods and Applications: AGU Reference Shelf 4, p. 157-175.

Hildenbrand, T. G., and Hendricks, J. D., 1995, Geophysical setting of the Reelfoot Rift and relations between rift structures and the New Madrid seismic zone, U.S. Geological Survey, Professional Paper 1538-E.

Hough, S. E., 2004, Scientific overview and historical context of the 1811-1812 New Madrid earthquake sequence, Annals of Geophysics, v. 47, n. 2/3, p. 523-537.

Idriss, I. M., and Boulanger, R. W., 2004, Semi-empirical procedures for evaluating liquefaction potential during earthquakes, Proc., 11th International Conference on Soil Dynamics and

Earthquake Engineering, and 3rd International Conference on Earthquake Geotechnical Engineering, D. Doolin et al., eds., Stallion Press, v. 1, p. 32-56.
Juang, C. H., and Jiang, T., 2000, Assessing probablistic methods for liquefaction potential evaluation, Soil Dynamics and Liquefaction 2000, GSP 107 (Proceedings GeoDenver), American Society of Civil Engineers, Reston, VA.
Moss, R. E. S., Seed, R. B., Kayen, R. E., Steward, J. P., Der Kiureghian, and Cetin, K. O., 2006, CPT-based probablistic and deterministic assessment of in-situ seismic soil liquefaction potential, Journal of Geotechnical & Geoenvironmental Engineering, v. 132, n. 8, p. 1032-1051.
Obermeier, S. F., 1989, The New Madrid earthquakes: an engineering-geologic interpretation of relict liquefaction features, U.S. Geological Survey, Professional Paper 1336-B.
Obermeier, S. F., 1996, Using liquefaction-induced features for paleoseismic analysis, *in* McCalpin, J. P., ed., Paleoseismology, Academic Press, San Diego, CA, p. 331-396.
Odum, J. K., Williams, R. A., Stephenson, W. J., Tuttle, M. P., Al-Shukri, H., 2016, Preliminary assessment of a previously unknown fault zone beneath the Daytona Beach sand blow cluster near Marianna, Arkansas, Seismological Research Letters, v. 87, n. 6, p. 1453-1464.
Prescott, J. R., and Hutton, J. T., 1994, Cosmic ray contributions to dose rates for luminescence and ESR dating: Large depths and long-term time variations, Radiation Measurements, v. 23, p. 497-500.
Al-Qadhi, O, 2010, Geophysical investigation of paleoseismological features in eastern Arkansas, USA: Ph.D dissertation, University of Arkansas at Little Rock, Little Rock, Arkansas, 235 p., plus Appendix A.
Al-Shukri H. J., Lemmer, R. E., Mahdi, H. H., and Connelly, J. B., 2005, Spatial and temporal characteristics of paleoseismic features in the southern terminus of the New Madrid seismic zone in eastern Arkansas, Seismological Research Letters, v. 76, p. 502-511.
Al-Shukri, H., Mahdi, H., and Tuttle, M., 2006, Three-dimensional imaging of earthquake-induced features with ground penetrating radar, near Marianna, Arkansas, Seismological Research Letters, v. 77, p. 505-513.
Al-Shukri, H., Mahdi, H., Al-Qadhi, O., and Tuttle, M.P., 2009, Spatial and temporal characteristics of paleoseismic features in the southern terminus of the New Madrid seismic zone in eastern Arkansas, Final Technical Report, Prepared for U.S. Geological Survey award 1434-07HQGR0069, 24 p.
Al-Shukri, H., Mahdi, H., Tuttle, M. P., Dyer-Williams, K., 2015, Geophysical and paleoseismic investigations of large sand blows along a northwest-oriented lineament near Marianna, Arkansas, Final Technical Report, Prepared for U.S. Geological Survey award G12AP20093, 31 p.
Reimer P. J., Bard, E., Bayliss, A., et al., 2013, INTCAL13 and marine13 radiocarbon age calibration curves 0-50,000 years cal BP, Radiocarbon, v. 55, n. 4, p. 1869-1887.
Robertson, P. K., 2004, Evaluating soil liquefaction and post-earthquake deformations using the CPT, Geotechnical and Geophysical Site Characterization, v.1 (Proc. ISC-2, Porto), Millpress, Rotterdam, p. 233-252.
Robertson, P. K., 2009, Interpretation of cone penetration tests: a unified approach, Canadian Geotechnical Journal, v. 46, n. 11, p. 1335-1355.
Saucier, R.T., 1977, Effects of the New Madrid earthquake series in the Mississippi alluvial valley, U.S. Army Corps of Engineers Waterways Experiment Station Miscellaneous Paper S-77-5, 10.

Schumm, S.A., and Spitz, W.J., 1996, Geological influences on the lower Mississippi River and its alluvial valley: Engineering Geology, v. 45, pp. 245-261.
Seed, H. B. and Idriss, I. M., 1971, Simplified procedure for evaluating soil liquefaction potential, Journal of the Soil Mechanics & Foundations Division (ASCE), v. 97 (SM9), p. 1249-1273.
Seed, H. B., and Idriss, I. M., 1982, Ground motions and soil liquefaction during earthquakes, Earthquake Engineering Research Institute, Berkley, 134 p.
Tuttle, M. P., 2001, The use of liquefaction features in paleoseismology: Lessons learned in the New Madrid seismic zone, central United States, Journal of Seismology, v. *5*, p. 361-380.
Tuttle, M. P., Schweig, E. S., Sims, J. D., Lafferty, R. H., Wolf, L. W., Haynes, M. L., 2002, The earthquake potential of the New Madrid seismic zone, Bulletin of the Seismological Society of America, v. 92, n. 6, p. 2080-2089.
Tuttle, M. P., Schweig, E., III, Campbell, J., Thomas, P. M., Sims, J. D., and Lafferty, R. H., III, 2005, Evidence for New Madrid earthquakes in A.D. 300 and 2350 B.C., Seismological Research Letters, v. 76, n. 4, p. 489-501.
Tuttle, M. P., Al-Shukri, H, and Mahdi, H., 2006, Very large earthquakes centered southwest of the New Madrid seismic zone 5,000-7,000 years ago, Seismological Research Letters, v. 77, n. 6, p. 664-678.
Tuttle, M. P., and Hartleb, R., 2012, Appendix E. Central and eastern U.S. paleoliquefaction database, uncertainties associated with paleoliquefaction data, and guidance for seismic source characterization, *in* The Central and Eastern U.S. Seismic Source Characterization for Nuclear Facilities, Technical Report, EPRI, Palo Alto, CA, U.S. DOE, and U.S. NRC, 135 p., plus database.
Tuttle, M. P., Hartleb, R., Wolf, L., and Mayne, P. W., 2019a, Paleoliquefaction studies and the evaluation of seismic hazard, Geosciences, v. 9, n. 7, 61 p, doi:10.3390/geosciences9070311.
Tuttle, M. P., Wolf, L. W., Dyer-Williams, K., Mayne, P. W., and Lafferty, R. H., et al., 2019b, Paleoliquefaction studies in moderate seismicity regions with a history of large earthquakes, U.S. Nuclear Regulatory Agency, NUREG/CR-7257, 450 p.
Tuttle, M. P., Wolf, L. W., Starr, M. E., Villamor, P., et al., 2019c, Evidence for large New Madrid earthquakes about A.D. 0 and B.C. 1050, Central United States, Seismological Research Letters, v. 90, n. 3, p. 1393-1406.
Wheeler, R. L., Omdahl, E. M., Dart, R. L., Wilkerson, G. D., and Bradford, R. H., 2003, Earthquakes in the central U.S., 1699-2002, U. S. Geological Survey, Geological investigations series I-2812.
Youd, T.L., et al., 2001, Liquefaction resistance of soils: Summary report from the 1996 NCEER and 1998 NCEER/NSF workshops on evaluation of liquefaction resistence of soils, Journal of Geotechnical and Geoenvironmental Engineering, v. 127, n. 10, p. 817-833.
Youd, T. L., and Idriss, I. M., 2003, Liquefaction resistance of soils: Summary report from the 1996 NCEER and 1998 NCEER/NSF workshops on evaluation of liquefaction resistance of soils: Closure and Errata, Journal of Geotechnical and Geoenvironmental Engineering, v. 129, n. 3, 285 p.

Bibliography of Related Publications

Al-Qadhi, O, 2010, Geophysical investigation of paleoseismological features in eastern Arkansas, USA: Ph.D dissertation, University of Arkansas at Little Rock, Little Rock, Arkansas, 235 p., plus Appendix A.

Al-Shukri H. J., Lemmer, R. E., Mahdi, H. H., and Connelly, J. B., 2005, Spatial and temporal characteristics of paleoseismic features in the southern terminus of the New Madrid seismic zone in eastern Arkansas, Seismological Research Letters, v. 76, p. 502-511.

Al-Shukri, H., Mahdi, H., and Tuttle, M., 2006, Three-dimensional imaging of earthquake-induced features with ground penetrating radar, near Marianna, Arkansas, Seismological Research Letters, v. 77, p. 505-513.

Al-Shukri, H., Mahdi, H., Al-Qadhi, O., and Tuttle, M.P., 2009, Spatial and temporal characteristics of paleoseismic features in the southern terminus of the New Madrid seismic zone in eastern Arkansas, Final Technical Report, Prepared for U.S. Geological Survey award 1434-07HQGR0069, 24 p.

Al-Shukri, H., Mahdi, H., Tuttle, M. P., Dyer-Williams, K., 2015, Geophysical and paleoseismic investigations of large sand blows along a northwest-oriented lineament near Marianna, Arkansas, Final Technical Report, Prepared for U.S. Geological Survey award G12AP20093, 31 p.

Tuttle, M. P., Al-Shukri, H, and Mahdi, H., 2006, Very large earthquakes centered southwest of the New Madrid seismic zone 5,000-7,000 years ago, Seismological Research Letters, v. 77, n. 6, p. 664-678.

Tuttle, M. P., and Hartleb, R., 2012, Central and eastern U.S. paleoliquefaction database, uncertainties associated with paleoliquefaction data, and guidance for seismic source characterization, Appendix E. *in* The Central and Eastern U.S. Seismic Source Characterization for Nuclear Facilities, Technical Report, EPRI, Palo Alto, CA, U.S. DOE, and U.S. NRC, 135 p. plus database.

Tuttle, M. P., Hussein, R., Al-Shukri, H, and Mahdi, H., Dyer-Williams, K., and Tucker, K., 2020, Investigating the earthquake potential of the Marianna source, East-Central Arkansas, Abstract, Geological Society of America, Joint 69th Annual Southeastern/55th Annual Northeastern Section Meeting (canceled due to Covid-19; abstract will be resubmitted for GSA 2020 Connects Online).